Article

Chinese Science Bulletin

Engineering Thermophysics

April 2013 Vol.58 No.11: 1325–1330
doi: 10.1007/s11434-012-5214-z

Characteristics of onset and damping in a standing-wave thermoacoustic engine driven by liquid nitrogen

QIU LiMin[1], LOU Ping[1], WANG Kai[1], WANG Bo[1,2], SUN DaMing[1], RAO JunFeng[1] & ZHANG XueJun[1*]

[1]*Institute of Refrigeration and Cryogenics, Zhejiang University, Hangzhou 310027, China;*
[2]*The 16th Research Institute of China Electronics Technology Group, Hefei 230043, China*

Received August 17, 2012; accepted November 14, 2012

We explore characteristics of onset and damping in a thermoacoustic engine (TE) driven by cryogens instead of conventional heat sources above the ambient temperature by a comprehensive study of a self-made standing-wave thermoacoustic engine driven by liquid nitrogen. The experiments verify the feasibility of enhancing the thermoacoustic oscillation at cryogenic temperatures. The onset temperature difference along the stack of the TE significantly decreases, compared with that of a conventional TE driven by high-temperature heat sources. The resonance frequency of the cryogen-driven TE is smaller than that of the heat-source-driven TE, mainly due to the lower average temperature of the working gas. Experiments and calculations show that the temperature discrepancy between onset and damping is partly caused by the linear temperature distribution along the stack before damping, together with the nonlinear distribution before onset. These results will contribute to a better understanding of thermoacoustic oscillation and to the recovery of the cold energy of cryogens.

thermoacoustic engine, cryogens, onset, damping

Citation: Qiu L M, Lou P, Wang K, et al. Characteristics of onset and damping in a standing-wave thermoacoustic engine driven by liquid nitrogen. Chin Sci Bull, 2013, 58: 1325–1330, doi: 10.1007/s11434-012-5214-z

A thermoacoustic engine (TE) is a novel type of heat engine which converts thermal energy into acoustic power via the thermoacoustic effect. With advantages such as having no moving parts, a high reliability, and its use of low-grade thermal energy, the TE has a promising prospect in the field of refrigeration and power generation [1–5].

It is indispensable to impose an adequate temperature gradient along the stack or the regenerator of the TE to realize self-oscillation. Conventionally, the TE absorbs heat from a heat source much hotter than the ambient temperature and expels heat to the ambience (i.e. a heat-source-driven thermoacoustic engine, HTE). In fact, from a thermodynamic point of view, it is possible to drive engines using the temperature gradient formed by a cold source below the ambient temperature and the ambience (i.e., a cold-source-driven thermoacoustic engine, CTE). Thermoacoustic oscillation at cryogenic temperatures has attracted attention since Taconis et al. [6] discovered the famous "Taconis oscillation" in 1949. Clement et al. [7] observed experimentally that the degrees of closure at the cold end and the diameter size of tubes affected the initial oscillation. Quantitative understanding was not achieved until Rott's theoretical studies [8,9], which were first validated experimentally by Merkli et al. [10]. Later Yazaki et al. [11,12] conducted experimental research on the stability curves and the frequency diagram of cryogenic thermoacoustic oscillation with helium gas. However, these studies mainly focus on eliminating or suppressing thermoacoustic oscillations at cryogenic temperatures, so as to avoid system instability. To our knowledge, Wheatley was the first to attempt to harness the thermoacoustic oscillation at cryogenic temperatures. He built a thermoacoustic oscillator in 1984, using liquid nitrogen as a heat sink to take the heat away from the cold heat exchanger [13]. The time development of the oscilla-

*Corresponding author (email: xuejzhang@zju.edu.cn)

tions was tested and the peak-to-peak maximum oscillation reached 11% of the ambient pressure. In 1992, Luck et al. [14,15] designed and built a thermoacoustic compressor with a solid piston, which achieved a maximum pressure amplitude of 3 kPa with no net work delivered. It should be noted that their work is very preliminary, without a detailed analysis of the thermoacoustic oscillation driven by cryogens. No more related research has been reported since then.

Cold energy resources are available and abundant, such as the energy stored in liquefied natural gas (LNG) and other liquid cryogens like liquid nitrogen and liquid oxygen. The cold energy should be fully used during gasification, although it is usually wasted due to low efficiency and the high cost of current technologies [16]. A good alternative to current practices of driving TEs using cryogens is to achieve the efficient conversion of heat to acoustic power for the purpose of cold-energy recovery of cryogens.

It is necessary to further enhance the thermoacoustic effects by developing a better understanding of thermoacoustic oscillation in the CTE. As a fundamental topic, the onset and damping behavior which characterizes the transitions in the condition of the working gas between the stationary and the periodic oscillating state deserves primary attention [17,18]. This study investigates a self-made standing-wave thermoacoustic engine driven by liquid nitrogen. Theoretical analysis based on thermoacoustic network theory [19,20] and experimental work were performed to study the onset and damping behaviors, including the onset temperature, the damping temperature, and the resonant frequency, and to further explore the reason for the discrepancy between the onset and damping temperature.

1 Apparatus

The experimental apparatus is sketched schematically in Figure 1. It consists of a standing-wave thermoacoustic engine (SWTE), a liquid nitrogen supply system, and a measurement system. The SWTE consists of the following parts: a hot tube, a hot heat exchanger, a stack, a cold heat exchanger, a resonator, and a reservoir. The stack is composed of a stainless steel screen with 18 meshes. High-purity nitrogen is charged as the working gas. The dimensions of the SWTE are listed in Table 1.

As shown in Figure 1, the chilled water flows through the hot heat exchanger to maintain the temperature T_h at about 280.5 K. The cold heat exchanger is cooled by liquid nitrogen, which is pressed out from the liquid-nitrogen tank by about 0.2 MPa high-pressure nitrogen. Four calibrated platinum resistance thermometers Pt-100 and one calibrated NiCr-NiSi thermocouple were installed to measure the temperature in the cold heat exchanger (T_c), in the middle of the stack (T_{mid}), at the inlet and outlet (T_{in} and T_{out}), and in the hot heat exchanger (T_h). The pressure p, as shown in Figure 1, was measured by a piezoelectric ceramic pressure sensor with an accuracy of ±0.3% and its influence on the accuracy of the temperature is negligible (±0.015% fs/K). Because the operating temperature of the sensor ranges from 233.15 to 423.15 K, a stainless-steel tube (120 mm in length) with an inner diameter of 11 mm and a wall thickness of 0.5 mm, was used to connect the TE and the sensor to ensure that the pressure sensor operates within the appropriate operating temperature range. A calculation shows that the tube has little influence on the pressure amplitude of the TE within 0.5%. In addition, the average mass flow rate of liquid nitrogen was measured with an accuracy of 0.01 g/s.

2 Results and analysis

2.1 Onset process

The onset and damping processes of a TE driven by liquid

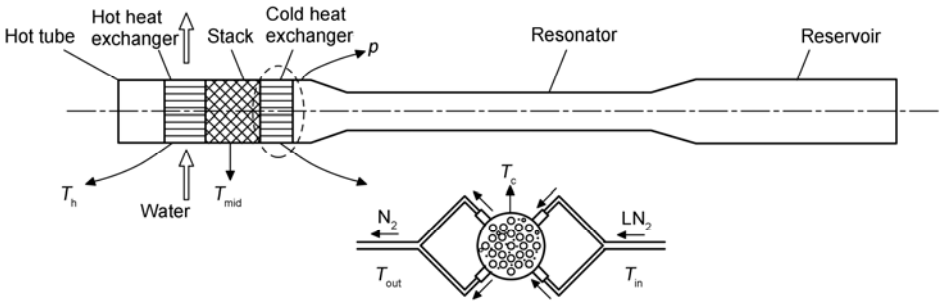

Figure 1 Schematic diagram of the SWTE driven by liquid nitrogen.

Table 1 Dimensions of the SWTE

	Hot tube	Hot heat exchanger	Stack	Cold heat exchanger	Resonator	Reservoir
Diameter (mm)	50	50	50	50	32	81
Length (mm)	70	80	60	50	860	860
Stack material			18# stainless steel screen			

nitrogen with a charging pressure of 0.6 MPa is shown in Figure 2. As the cooling system starts at time 0, the inlet temperature T_{in} decreases to 85.6 K within a short period of time. T_c, T_{out}, and T_{mid} gradually decrease and T_h remains stable at 280±0.5 K. The flow rate of liquid nitrogen is adjusted at Time 1 and Time 2. When T_c approaches the onset temperature, the mass flow of liquid nitrogen is adjusted to 2.23 g/s and the corresponding cool-down rate is controlled at 0.01 K/s.

When the temperature at the cold heat exchanger reaches 141.57 K, the self-oscillation starts. Simultaneously, the pressure amplitude jumps to 27 kPa and T_{mid} decreases sharply. The hot heat exchanger temperature T_h also decreases by about 1 K. This is mainly because when the oscillation starts convection replaces conduction as the major mechanism of axial heat transfer in the stack. Heat flow from the cold heat exchanger to the hot heat exchanger occurs within a short time period, as a result of which the temperature in the middle of stack decreases. After onset, the oscillation of the system tends to be stable, as a result of the energy balance between the cold power input and the oscillation loss.

2.2 Onset temperature difference

To select an appropriate heat source conveniently for application, we introduce the concept of "onset temperature difference" (i.e. the temperature difference across the stack T_h–T_c). Figure 3 shows the relationship between the onset temperature difference and charging pressure for the CTE and the HTE. Compared with the HTE, the CTE requires a smaller temperature difference to oscillate. For instance, with nitrogen at 0.6 MPa, the onset temperature difference of the CTE is only 138.43 K, i.e. 31% lower than that of the HTE. Moreover, as the charging pressure increases, the variation in the onset temperature difference of the CTE tends to be gradual, compared with the HTE, which means

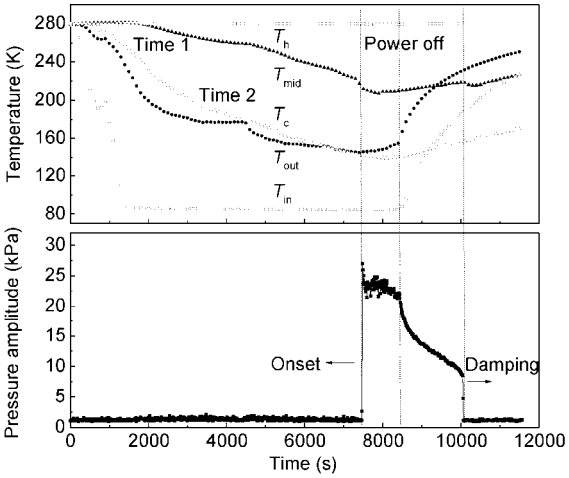

Figure 2 Variation in pressure amplitude and temperatures of the CTE (0.6 MPa, N_2).

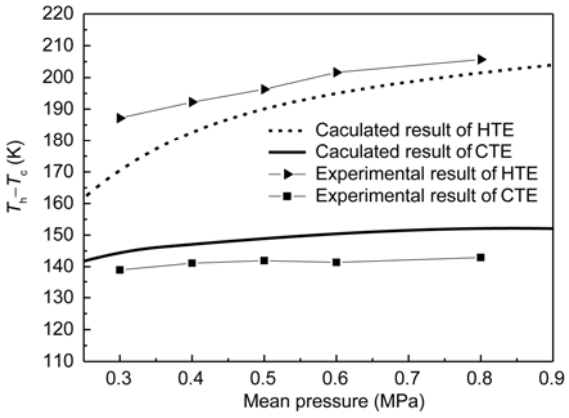

Figure 3 Relationship between the onset temperature difference and the charging pressure in the CTE and the HTE.

that the CTE will achieve a higher pressure amplitude with higher charging pressure. In addition, we perform a calculation based on the thermoacoustic network theory, as shown in Figure 3. The calculation and experimental results show a similar tendency.

To further analyze the reason for the discrepancy in the onset temperature difference between the CTE and the HTE, we define a dimensionless parameter $\tau = \frac{c}{4\pi fl}(\frac{T_h}{T_c} - 1)$, where c is the speed of sound, f is the operating frequency, and l is the length of the stack. It represents the critical temperature gradient within the stack when oscillation starts. It is a function of the hydraulic radius R_h and the thermal boundary layer thickness δ_κ of the stack and is minimized mostly when $R_h / \delta_\kappa \approx 2$ [21]. On account of the different temperature of the driving source, the thermal boundary layer thickness δ_κ of the working gas in the stack in the CTE is different from that of the HTE. Thus, the values of τ for the CTE and HTE are also different. The dimensionless parameter τ of the HTE and the CTE is plotted against R_h / δ_κ in Figure 4. For the CTE and the HTE, the variation trend of τ is the same, and the τ for the CTE ranges from 0.6 to 1, while the τ for the HTE ranges from 0.45 to 0.7. According to the definition of τ, it can be rewritten as $\tau = \frac{(T_h - T_c)c}{T_c 4\pi fl}$. It is obvious that the onset temperature difference of the CTE is smaller than the HTE because of its smaller denominator, which is proportional to T_c.

Figure 5 shows the relationships between R_h / δ_κ and the charging pressure for the HTE and the CTE. The difficulty of onset is different for these two kinds of engines, for the same charging pressure. When $R_h / \delta_\kappa = 2$, the CTE has an optimal charging pressure of 0.06 MPa to minimize the dimensionless parameter τ, whereas it is 0.12 MPa for the HTE.

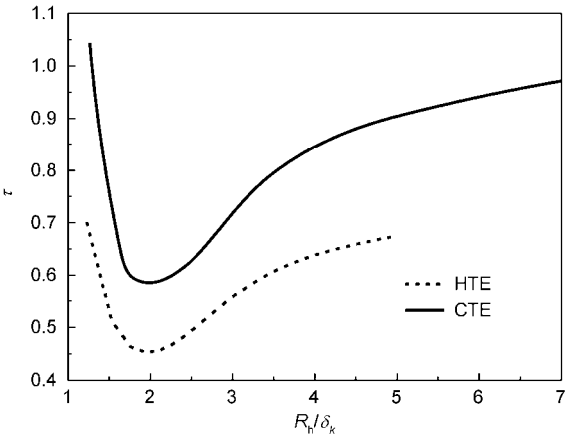

Figure 4 Relationship between τ and R_h/δ_k of the CTE and the HTE.

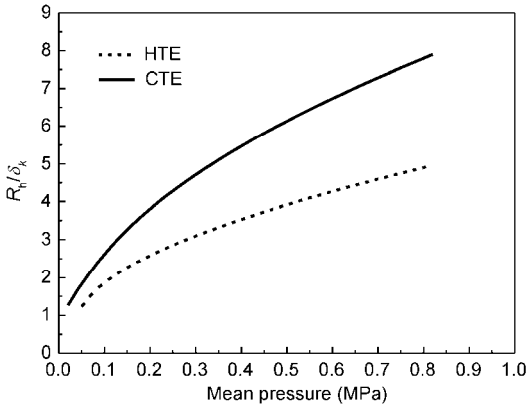

Figure 5 Relationship between R_h/δ_k and charging pressure of the CTE and the HTE.

2.3 Resonance frequency

The resonance frequency primarily depends on the system dimensions, the fluid type, and the temperature of the working gas. Figure 6 shows the frequency of the HTE and the CTE with a variety of charging pressures. Compared with the HTE, the frequency of the CTE is smaller. For instance, with nitrogen at 0.6 MPa, the onset frequency of the CTE is 57.15 Hz, whereas that of the HTE is 60.26 Hz. According to the equations $f = c / \lambda$ and $c = \sqrt{\gamma R_g T}$, where γ is the ratio of the isobaric to isochoric specific heats and equals 1.4 for nitrogen, R_g is the gas constant, T is the temperature of the working gas, the resonance frequency should only be proportional to the average temperature of working gas for a TE with a fixed structure. Because the gas temperature in the CTE is lower than in the HTE, the frequency decreases. As shown in Figure 6 the trends are basically consistent with the theoretical calculation.

2.4 Damping behavior

The damping behavior of the CTE was also investigated. As

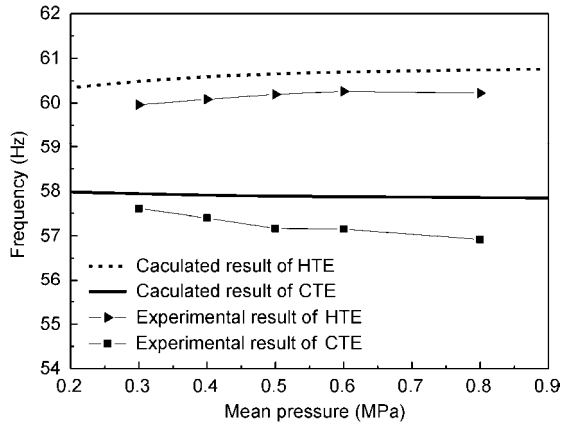

Figure 6 Relationship between the operating frequency and the charging pressure of the CTE and the HTE.

shown in Figure 2, the valve of the cooling system is closed slowly to make the temperature in the cold heat exchanger rise gradually. Although the system continues to oscillate, the pressure amplitude slowly decreases. The oscillation does not disappear abruptly until the temperature in the cold heat exchanger has reached 157.1 K. Figure 7 plots the pressure amplitude of the CTE with a filling pressure of 0.6 MPa as a function of the temperature in the cold heat exchanger. Obviously, a "hysteretic loop" [22] which exists in the HTE is also present in the CTE. When the temperature of the cold heat exchanger reaches 141.57 K, the system starts to oscillate and pressure amplitude suddenly jumps. Then the pressure amplitude decreases gradually as T_c rises, and, when temperature reaches 157.1 K, the pressure amplitude jumps from 8.42 to 1.16 kPa. It is clear that the hysteretic loop is formed by the two vertical lines and the two approximately horizontal lines. There is a temperature difference of 15.53 K between the onset and the damping temperatures.

The temperature discrepancy between onset and damping is generally attributed to nonlinearity during the state transitions. In fact, it is also affected by the temperature

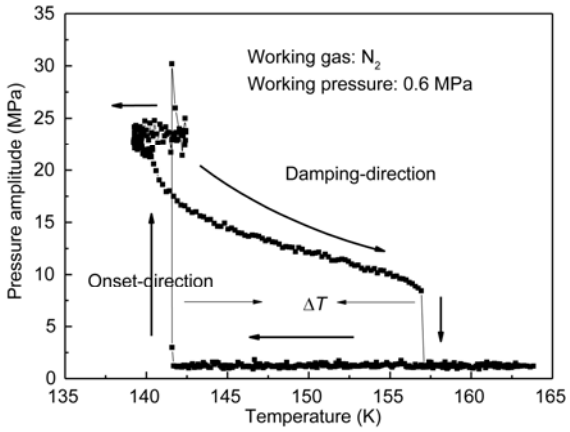

Figure 7 Dynamic onset and damping process of the CTE (0.6 MPa, N_2).

distribution within the stack. Here, to simplify the analysis, we investigate the effect of temperature in the middle of the stack on the onset and damping behaviors. Consider the CTE as an example. Figure 8 shows the variation in the temperature in the middle of the stack during onset and damping. The dimensionless length of the stack is defined as $L_d = x/l$, where x is the length measured from the cold end to the hot end of the stack, l is the length of the stack (i.e., for the location of the middle of stack, $L_d = 0.5$). The dimensionless temperature T_d is defined as $T_{mid} = T_h - T_d(T_h - T_c)$, where T_{mid}, T_h, and T_c are the temperatures in the middle of the stack, the hot heat exchanger, and the cold heat exchanger, respectively. As shown in Figure 8, before onset, because the main mechanism of heat transfer in the TE is conduction, T_d = 0.445 and the temperature in the stack is not linearly distributed. After onset, as the working gas starts to oscillate, convection replaces conduction as the main mechanism, which largely enhances the heat transfer in the axial direction. Consequently, the temperature distribution along the stack becomes linear.

Figure 9 shows the onset temperature difference as a function of the temperature distribution in the stack. As T_d rises (i.e. the temperature in the middle of the stack decreases), the onset temperature difference appears to increase at first and then to decrease. When T_d = 0.445, the onset temperature difference is 153.0 K, which is 0.5 K larger than that when the stack temperature is linearly distributed (i.e. T_d = 0.5). This shows that the onset temperature difference decreases when the oscillation starts in the system and temperature distribution in the stack tends to be linear. It is assumed that the temperature discrepancy between onset and damping is partly caused by the linear temperature distribution before oscillation disappears, together with the nonlinear temperature distribution before oscillation starts.

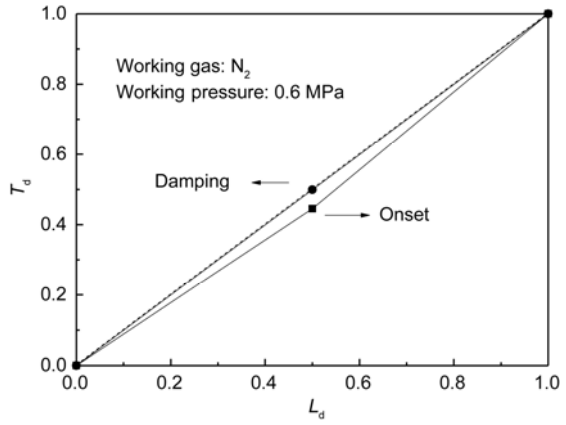

Figure 8 Dimensionless temperature variation in the middle of the stack of the CTE at onset.

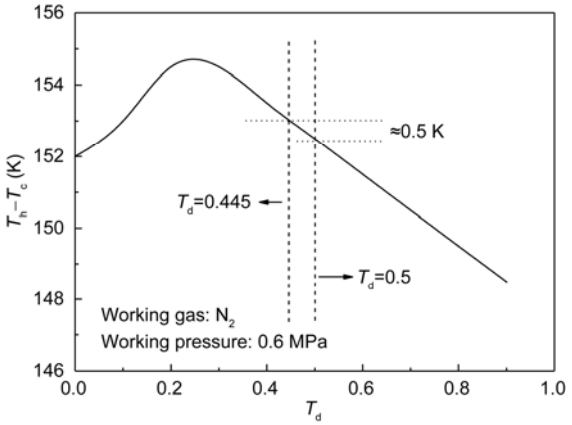

Figure 9 Effect of the temperature in the middle of stack on the onset temperature.

3 Conclusions

A standing-wave thermoacoustic engine driven by liquid nitrogen was tested to investigate the onset and damping characteristics. The experiments further verify the feasibility of thermoacoustic engines driven by cryogens. For the same dimensionless parameter, the onset temperature difference of the CTE is much lower than that of the HTE. For instance, with nitrogen at 0.6 MPa, the onset temperature difference of the CTE is only 138.43 K, which is only 68% of that of the HTE. Furthermore, because of the lower average temperature of the working gas, the resonance frequency of the CTE is smaller than that of the HTE. Theoretical analysis based on the thermoacoustic network shows agreement with experiments in predicting the onset temperature difference and the frequency for the thermoacoustic engine. In addition, the onset and damping hysteretic loop is first found in the thermoacoustic engine driven by cryogen. Computed results demonstrate that one of the reasons for the temperature difference between onset and damping is the linear temperature distribution in the stack when damping, together with the nonlinear distribution before onset.

It should be noted that the TE can realize self-oscillation with a limited temperature gradient imposed only by a cold source and the ambient temperature. It would be possible to obtain a much more intense thermoacoustic oscillation if the TE were driven by cold sources like liquid nitrogen and heat sources above the ambient temperature, e.g., low-grade thermal energy, simultaneously. This is the subject of current research.

This work was supported by the National Science Funds for Distinguished Young Scholars (50825601) and the National Basic Research Program of China(2010CB227303). The authors thank Dr. R. Radebaugh and Prof.de Waele for helpful discussions.

1 Backhaus S, Swift G W. A thermoacoustic Stirling heat engine. Nature, 1999, 399: 335–338
2 Qiu L M, Sun D M, Yan W L, et al. Investigation on a thermoacous-

tically driven pulse tube cooler working at 80 K. Cryogenics, 2005, 45: 380–385
3 Chen G B, Tang K, Jin T. Advances in thermoacoustic engine and its application to pulse tube refrigeration. Chin Sci Bull, 2004, 49: 1319–1328
4 Backhaus S, Tward E, Petach M. Traveling-wave thermoacoustic electric generator. Appl Phys Lett, 2004, 85: 1085–1087
5 Wu Z H, Man M, Luo E C, et al. Experimental investigation of a 500 W traveling-wave thermoacoustic electricity generator. Chin Sci Bull, 2011, 56: 975–1977
6 Taconis K W, Beenakker J J M, Nier A O, et al. Measurements concerning the vapor-liquid equilibrium of solutions of He^3 in He^4 below 2.19 K. Phys Rev, 1949, 75: 1966
7 Clement J R, Gaffney J. Thermal oscillation in low temperature apparatus. Adv Cryo Eng, 1954, 1: 302–306
8 Rott N. Damped and thermally driven acoustic oscillations in wide and narrow tubes. Z Angew Math Phys, 1969, 20: 230–243
9 Rott N. Thermally driven acoustic oscillations. Part 2: Stability limit for helium. Z Angew Math Phys, 1973, 24: 54–72
10 Merkli P, Thomann H. Thermoacoustic effects in a resonance tube. J Fluid Mech, 1975, 70: 161–177
11 Yazaki T, Tominaga A, Narahara Y. Experiments on thermally driven acoustic-oscillations of gaseous helium. J Low Temp Phys, 1980, 41: 45–60
12 Yazaki T, Sugioka S, Mizutani F, et al. Nonlinear dynamics of a forced thermoacoustic oscillation. Phys Rev Lett, 1990, 64: 2515–2518
13 Wheatley J, Hofler T, Swift G W, et al. Understanding some simple phenomena in thermoacoustics with applications to acoustical heat engines. Am J Phys, 1985, 53: 147–162
14 Luck H, Trepp C. Thermoacoustic oscillations in cryogenics. Part 1: Basic theory and experimental verification. Cryogenics, 1992, 32: 690–697
15 Luck H, Trepp C. Thermoacoustic oscillations in cryogenics. Part 2: Applications. Cryogenics, 1992, 32: 698–702
16 Szargut J, Szczygiel l. Utilization of the cryogenic exergy of liquid natural gas (LNG) for the production of electricity. Energy, 2009, 34: 827–837
17 Atchley A A. Analysis of the initial buildup of oscillations in a thermoacoustic prime mover. J Acoust Soc Am, 1994, 95: 1661–1664
18 Qiu L M, Sun D M, Tan Y X, et al. Effect of pressure disturbance on onset processes in thermoacoustic engine. Energ Convers Manage, 2006, 47: 1383–1390
19 Swift G W. Thermoacoustics: A Unifying Perspective for Some Engines and Refrigerators. Sewickley, PA: Acoustical Society of America Publishers, 2002
20 Lai B H, Qiu L M, Li Y F, et al . Simulation of the onset process of standing wave thermoacoustic engine using thermoacoustic network theory (in Chinese). J Zhejiang Univ, 2011, 45: 1130–1135
21 Arnott W P, Belcher J R, Raspet R, et al. Stability analysis of a helium-filled thermoacoustic engine. J Acoust Soc Am, 1994, 96: 370–375
22 Chen G B, Jin T. Experimental investigation on the onset and damping behavior of the oscillation in a thermoacoustic prime mover. Cryogenics, 1999, 39: 843–846